AD-A146 052 STRUCTURAL STUDIES OF SPUTTERED MOS(2) FILMS BY ANGLE-RESOLVED PHOTOELECT..(U) AEROSPACE CORP EL SEGUNDO CA CHEMISTRY AND PHYSICS LAB 1/1

UNCLASSIFIED P D FLEISCHAUER ET AL. 06 SEP 84 F/G 20/2 NL

END
DATE FILMED
10 84
DTIC

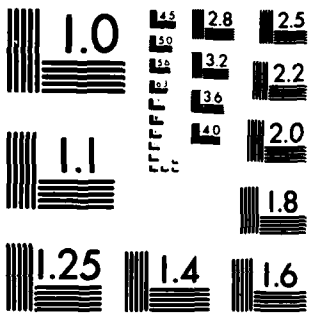


MICROCOPY RESOLUTION TEST CHART
NATIONAL BUREAU OF STANDARDS-1963-A

REPORT SD-TR-84-27

(12)

AD-A146 052

# Structural Studies of Sputtered $MoS_2$ Films by Angle-Resolved Photoelectron Spectroscopy

PAUL D. FLEISCHAUER and L. U. TOLENTINO
Chemistry and Physics Laboratory
Laboratory Operations
The Aerospace Corporation
El Segundo, Calif. 90245

6 September 1984







Prepared for
SPACE DIVISION
AIR FORCE SYSTEMS COMMAND
Los Angeles Air Force Station
P.O. Box 92960, Worldway Postal Center
Los Angeles, Calif. 90009

This report was submitted by The Aerospace Corporation, El Segundo, CA 90245, under Contract No. F04701-83-C-0084 with the Space Division, P.O. Box 92960, Worldway Postal Center, Los Angeles, CA 90009. It was reviewed and approved for The Aerospace Corporation by S. Feuerstein, Director, Chemistry and Physics Laboratory. Lieutenant Charles C. Neidhart, SD/YKXL, was the project officer for the Mission-Oriented Investigation and Experimentation (MOIE) program.

This report has been reviewed by the Public Affairs Office (PAS) and is releasable to the National Technical Information Service (NTIS). At NTIS, it will be available to the general public, including foreign nationals.

This technical report has been reviewed and is approved for publication. Publication of this report does not constitute Air Force approval of the report's findings or conclusions. It is published only for the exchange and stimulation of ideas.

Charles C. Neidhart

Charles C. Neidhart, Lt, USAF
Project Officer

Joseph Hess, GM-15, Director,
West Coast Office, AF Space
Technology Center

UNCLASSIFIED

SECURITY CLASSIFICATION OF THIS PAGE (When Data Entered)

| REPORT DOCUMENTATION PAGE | | READ INSTRUCTIONS BEFORE COMPLETING FORM |
|---|---|---|
| 1. REPORT NUMBER<br>SD-TR-84-27 | 2. GOVT ACCESSION NO.<br>AD-A146 052 | 3. RECIPIENT'S CATALOG NUMBER |
| 4. TITLE (and Subtitle)<br>Structural Studies of Sputtered $MoS_2$ Films by Angle-Resolved Photoelectron Spectroscopy | | 5. TYPE OF REPORT & PERIOD COVERED<br>6. PERFORMING ORG. REPORT NUMBER<br>TR-0084(4945-03)-3 |
| 7. AUTHOR(s)<br>Paul D. Fleischauer and Lucio U. Tolentino | | 8. CONTRACT OR GRANT NUMBER(s)<br>F04701-83-C-0084 |
| 9. PERFORMING ORGANIZATION NAME AND ADDRESS<br>The Aerospace Corporation<br>El Segundo, California 90245 | | 10. PROGRAM ELEMENT, PROJECT, TASK AREA & WORK UNIT NUMBERS |
| 11. CONTROLLING OFFICE NAME AND ADDRESS<br>Space Division<br>Los Angeles Air Force Station<br>Los Angeles, Calif. 90009 | | 12. REPORT DATE<br>6 September 1984<br>13. NUMBER OF PAGES<br>22 |
| 14. MONITORING AGENCY NAME & ADDRESS(if different from Controlling Office) | | 15. SECURITY CLASS. (of this report)<br>Unclassified<br>15a. DECLASSIFICATION/DOWNGRADING SCHEDULE |

16. DISTRIBUTION STATEMENT (of this Report)

Approved for public release; distribution unlimited.

17. DISTRIBUTION STATEMENT (of the abstract entered in Block 20, if different from Report)

18. SUPPLEMENTARY NOTES

19. KEY WORDS (Continue on reverse side if necessary and identify by block number)

Solid lubrication
Molybdenum disulfide
Photoelectron spectroscopy, angle resolution

20. ABSTRACT (Continue on reverse side if necessary and identify by block number)

$MoS_2$ films were deposited by rf sputtering on both single-crystal molybdenite and steel substrates to assess the effects of varying preparation conditions on film properties. They were then examined by angle-resolved x-ray photoelectron spectroscopy, which provided information on the orientation of the layered crystal substrate, on the film layers immediately adjacent to the substrate (within 1-10 nm), and on thicker, macroscopic films composed of relatively large crystallites (approximately 70-200 nm).

DD FORM 1473 (FACSIMILE)

UNCLASSIFIED

SECURITY CLASSIFICATION OF THIS PAGE (When Data Entered)

19. KEY WORDS (Continued)

20. ABSTRACT (Continued)

For the 4.3-nm-thick films deposited on the crystal's basal-plane surface, the angular dependence of the photoelectron emission is the same as the substrate's, indicating preferred orientation within such films. Angular distribution studies for thicker films on steel substrates are consistent with previous Auger electron spectroscopy results and confirm the presence of oxide films of different thickness on lubricant films with varying orientations. The angle-dependence data were fit to models that describe the structure and composition of the films' surfaces.

## PREFACE

The authors thank R. I. Christy of Hughes Aircraft Company for preparing the thick films; R. Bauer for preparing the thin films; J. L. Childs for making many of the XPS measurements; and Drs. P. A. Bertrand and G. W. Stupian for many helpful discussions related to the XPS data and attenuation calculations.

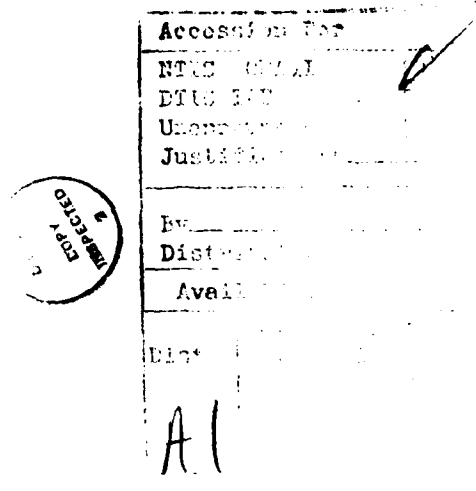

CONTENTS

## FIGURES

# I. INTRODUCTION

The chemical, structural, and tribological properties of sputtered molybdenum disulfide ($MoS_2$) films have been studied extensively.[1-7] In general, the lubrication properties of films improve as the stoichiometries of the films approach that of pure $MoS_2$. Specific results of surface analyses and microscopy have demonstrated that sputter-deposited films can have substantially different reactivities (i.e., oxidation chemistries) and different endurance lives during standard sliding wear tests. Auger electron spectroscopy (AES) and x-ray photoelectron spectroscopy (XPS) measurements have been used to formulate a descriptive model of $MoS_2$ film oxidation that is based on the geometrical orientation of crystallites composing the films with respect to the plane of the substrate surface.[5,7] Calculations of AES and XPS peak intensity ratios showed that 200-nm-thick films oriented with their basal planes parallel to the substrate plane are oxidized in humid air to a depth of only 1.0 to 1.5 nm, whereas films with random crystallite orientations are oxidized to depths exceeding 30 nm.[7] Crystallite orientation has also been applied to describe variations in wear properties of the films.[5] It was proposed that optimal films would have crystallites oriented parallel to the substrate surface, an orientation that would extend throughout the depth of the film from the initial layers in contact with the substrate out to the outer surface in contact with the environment. Achieving such preferred orientation requires proper bonding to the substrate and careful control of the deposition conditions so that the films have uniform structures.

The primary objective of this work is to determine the bonding and deposition conditions that result in properly oriented films on substrates of practical importance, such as bearing steels. To achieve this goal it was first necessary to develop a convenient technique for examining the films' interfacial layers and crystallite structures and to correlate the examination results with the electron distributions between the substrate metal and the sulfur or molybdenum atoms of the film. The correlation will determine the strengths and geometrical arrangement of the bond between the two constituents.

Angle-resolved XPS or ultraviolet photoelectron spectroscopy (UPS), coupled with appropriate shielding calculations, can provide the required information on electron distribution and atomic arrangement. Our preliminary measurements of XPS peak intensities as a function of the angle the electron path makes with the sample plane—takeoff angle—for various $MoS_2$ samples, verify the presence of oxide layers of different thicknesses on different types of sputtered $MoS_2$ films, demonstrate the possibility of obtaining oriented-interface films by sputter deposition, and identify oxidation of the film-substrate interface as an influential process during deposition.

## II. EXPERIMENTAL PROCEDURES

Films of $MoS_2$ were prepared with one of two different rf diode sputtering instruments operating at 2 kW with a frequency of 13.56 MHz and an argon pressure ranging from 1.33 to 2.1 Pa. The 200-nm-thick films were prepared from two different sputtering targets (different vendors) on C1018 steel substrates.[5,6] The targets were made from hot-pressed $MoS_2$ powder (99.9 percent pure), were 254 mm in diameter, and were bonded to copper plates. The specimens to be coated were located 25.4 mm below the target on a grounded block. A 5-kVA dc power supply was used to sputter etch-clean the samples before coating. These films were analyzed extensively by AES and XPS after storage in air at 0 percent relative humidity for 9 to 12 months.[7] The films were stored an additional 5 months under the same conditions before the angle-resolved XPS measurements reported here were made. Thinner films, ranging from ~ 4.3 to ~ 17 nm in thickness, were prepared in-house on molybdenite single-crystal or 440C steel substrates with a sputtering apparatus similar to that used for the thicker films but with the following differences: a gas purifier was installed in the argon supply line; a shutter was incorporated in the chamber, and the 152.4-mm-diam $MoS_2$ target was conditioned by presputtering on the shutter for 45 to 50 min; the chamber was evacuated to a pressure of $1.6 \times 10^{-3}$ Pa before sputtering; the argon pressure during sputtering was 2.1 Pa; and the sputtering rate was ~ 20 $nm \cdot min^{-1}$ for an rf power density of 2 $W \cdot cm^{-2}$. Single-crystal substrates, ~ 0.5 mm thick, were cleaved from a thicker specimen and placed on the substrate table of the sputtering system immediately before chamber evacuation. The $MoS_2$ film was deposited onto the basal plane of the crystal. Stainless-steel substrates were polished optically flat to a mirror finish.

X-ray photoelectron spectra were obtained with a GCA/McPherson ESCA-36 spectrometer modified by the addition of a position-sensitive, multichannel detector,[8] which increases the signal-to-noise ratio and decreases considerably the time to obtain a spectrum, thereby enabling relatively weak signals to be measured at low takeoff angles. Figure 1 diagrams the geometry

of the sample in relation to the incident x-ray beam and the emitted electron path. Electrons are emitted over a solid angle of $2\pi$ steradians, but the spectrometer slit defines a small, approximately 0.7° acceptance aperture. The smaller the takeoff angle $\theta$ (the angle that the path of the analyzed electrons makes with the sample surface), the greater is the relative enhancement of signals from layers on the sample's outermost surface.[9]

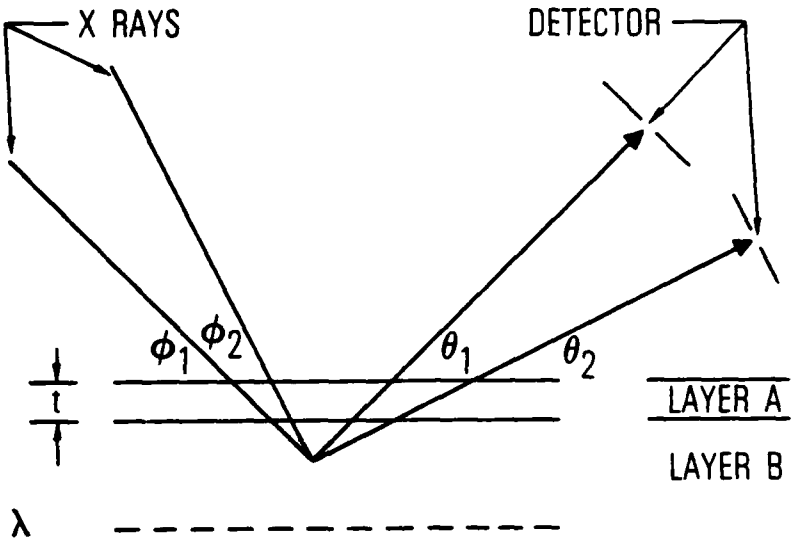


Fig. 1. Schematic of arrangement for angle-dependent XPS measurements. $\theta$ is the takeoff angle for electrons that enter the analyzer slit; $\phi$ is the angle between the x-ray beam and the surface.

Freshly cleaved molybdenite single crystals were examined by the angle-resolved technique to provide references for subsequent measurements and to establish the technique's feasibility.

## III. ANGLE-RESOLVED SPECTRA

Standard XPS measurements are made with a constant takeoff angle, say, 45°, and produce a spectrum like that of the basal plane of a molybdenite crystal (Fig. 2). Additional information concerning the electron orbitals involved in the photoelectron transition and any layering of the atoms composing the surface under analysis can be obtained by measuring XPS or UPS spectra at different takeoff angles.[9,10] Here, angular variations in the intensities of XPS peaks are used to characterize the crystallites of $MoS_2$ films as being oriented with their basal planes parallel to the substrate surface or in a random configuration, and to characterize the oxidation processes on these different types of film.

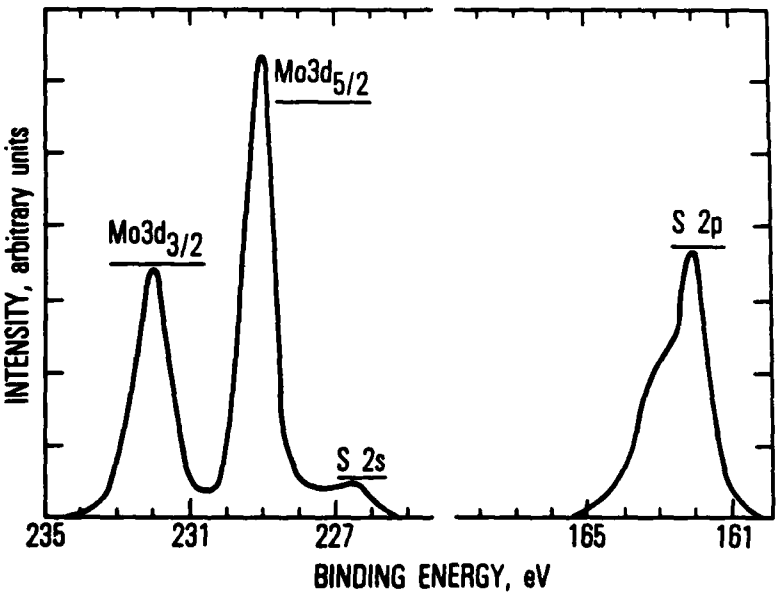


Fig. 2. XPS spectrum of $MoS_2$ single crystal (molybdenite).

Changes occurring in a material's chemistry can be determined from the values of the binding energies of peak maxima, data on peak shape, and ratios of peak intensities.[5-7] Such changes could be associated with adsorption onto, reaction of, or diffusion into the surface. Some information on depth, for example, approximate $MoS_2$ film oxidation depth, can be determined from calculations of emitted-electron attenuation caused by scattering by atoms that overlay the emitting atom and from measurements of such attenuations for electrons of different energies.[7] A generalized expression for emission of a film of substance B covered by an overlayer of substance A is given in Eq. (1):

$$I_{x(B)} = K\lambda_x \exp(-t_2/\lambda_x) [1 - \exp(-t_1/\lambda_x)] \quad (1)$$

where $t_1$ is the thickness of the emitting layer (B), $t_2$ is the thickness of the overlayer (A), $\lambda_x$ is the escape depth for the electrons emitted from element x, and K contains terms for the excitation cross section, the number of emitting atoms, and the spectrometer analyzer. Equation (1) is valid for the case when electrons emitted along the surface normal are analyzed. More precise depth information can be obtained if the sample is rotated so that the takeoff angle is less than 90°; then the apparent layer thickness, the distance into the surface from which electrons may escape, must be adjusted to account for the detection angle. The adjusted thickness t' is given by:

$$t' = t/\sin\theta \quad (2)$$

where $\theta$ (see Fig. 1) is the takeoff angle from the surface analyzed. Different forms of Eq. (1) will be used in subsequent sections of this report to treat different physical/chemical situations, such as a layer of oxide on top of $MoS_2$ or the layering of S and Mo atoms in pure $MoS_2$ and in $MoS_2$ thin films.

## IV. OXIDATION OF 200-nm-THICK FILMS

Oxidation of $MoS_2$ films produces $MoO_3$ either throughout the bulk of the film, for films with randomly oriented crystallites (designated Type I films), or as a thin layer on the film's surface, for planar-oriented films (Type II).[5,7] The formation of $MoO_3$ shifts the Mo3d XPS peaks approximately 3 eV to higher binding energy. The value of this shift is, within the resolution of our spectrometer, the same as the value of the $3d_{5/2}$-$3d_{3/2}$ doublet splitting energy. A three-peaked spectrum results for a partially oxidized film, as indicated in Fig. 3(c). The relative amounts of oxide and sulfide within the analysis depth of a typical film can be calculated from the XPS spectra, using the crystal spectrum (Fig. 2) as a reference. The integrated intensity ratio for the $3d_{5/2}$-to-$3d_{3/2}$ peaks of molybdenite is 1.55:1, which agrees with the theoretical value of 1.5:1. The peak-to-peak ratio is approximately 1.8:1. The analogous peak-to-peak ratio for a fully oxidized film is 1.51:1. Using these ratios and assuming the presence of only two Mo-containing substances in a partially oxidized film, one can calculate the ratio of Mo(IV) to Mo(VI), or $MoS_2$ to $MoO_3$, for any film. The data of Fig. 3 evidence that these ratios vary as a function of the takeoff angle of analysis, especially for Type II films. Type II films are much less oxidized than Type I after 1.5 years' storage in dry air, and the strength of the sulfide signal increases significantly relative to that of the oxide as the takeoff angle approaches 90 deg, meaning that the thickness of the oxide layer on the film's surface is comparable to the electron-escape depth.

The oxygen spectra for partially oxidized $MoS_2$ films are composed of at least two peaks, one for oxide oxygen ($O^{2-}$) at a binding energy of ~ 531 eV and one for adsorbed oxygen (or OH) at ~ 532 eV. Changes in the relative intensities of the oxygen peaks as the takeoff angle is varied provide another indication of the oxide (presumably $MoO_3$) layer thickness. Normally, the closer the takeoff angle is to the surface normal, the greater is the strength of the oxide signal relative to that of the adsorbed layer, because the adsorbed layer is presumed to cover the oxide or sulfide or both.[11] The

spectra of Fig. 4 show that the situations for Types I and II $MoS_2$ films differ: Type I films exhibit the conventional behavior, but Type II films behave oppositely, the oxide signal decreasing relative to that of the adsorbed oxygen as θ increases. The spectral variations for Type II films are consistent with a very thin, possibly hydrated or discontinuous layer of oxide on the sulfide surface, with adsorbed oxygen or water throughout the oxide layer and even between the oxide and sulfide.

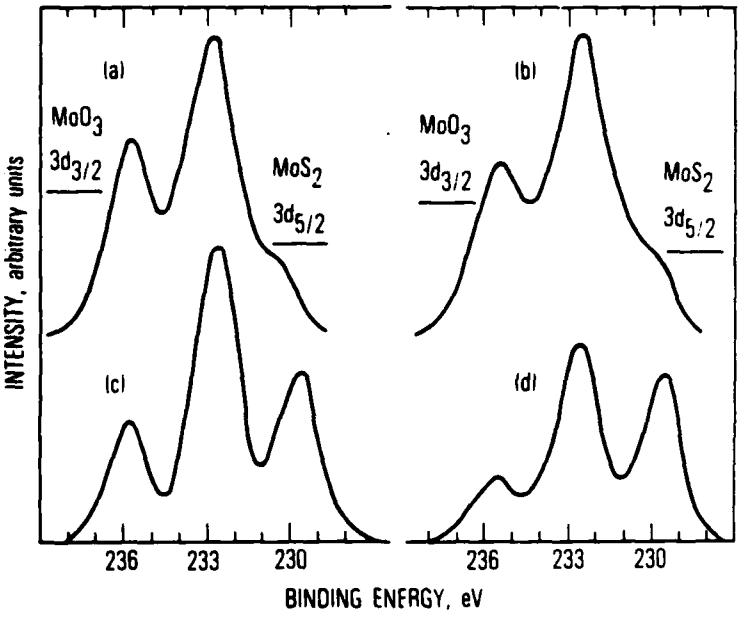


Fig. 3. Molybdenum XPS spectra at different angles of 200-nm-thick, rf sputter-deposited $MoS_2$ films after storage for 1.5 years in dry air: (a) Type I film at 30°, Mo(IV):Mo(VI) ≈ 0.2; (b) Type I film at 64°, Mo(IV):Mo(VI) ≈ 0.3; (c) Type II film at 30°, Mo(IV):Mo(VI) ≈ 0.9; and (d) Type II film at 60°, Mo(IV):Mo(VI) ≈ 1.7.

Figure 5, a plot of the ratios of film constituents as functions of the takeoff angle, depicts the gross differences between the two types of films. The sulfide [Mo(IV)] to oxide [Mo(VI)] ratio for Type II films is almost ten times greater than that for Type I films. The line marked "calculated for 1.2-nm $MoO_3$" film was obtained by the use of a variation of Eq. (1) together with the following assumptions: (1) the 1.2-nm-thick $MoO_3$ layer was assumed

to be continuous and 100 percent oxide; (2) the thickness of the $MoS_2$ layer was assumed to be much greater than $\lambda_{Mo}$, the escape depth of Mo electrons; (3) the escape depths for Mo(IV) and Mo(VI) electrons were assumed to be equal, as were the other parameters in the proportionality constant K; and (4) the effects of adsorbed oxygen were ignored. If appropriate substitutions are made in Eq. (1), the ratio of Mo(IV) emission intensity to Mo(VI) intensity for $\theta = 90°$ can be expressed as follows:

$$\frac{Mo(IV)}{Mo(VI)} = \frac{\exp(-t_2/\lambda)}{1 - \exp(-t_2/\lambda)} = \frac{1}{\exp(t_2/\lambda) - 1} \tag{3}$$

where $t_2$ is the thickness of the $MoO_3$ layer. The variation in this ratio with takeoff angle $\theta$ can be expressed by combining Eqs. (2) and (3) to give

$$\frac{Mo(IV)}{Mo(VI)} = \frac{1}{\exp(t_2/\lambda \sin \theta) - 1} \tag{4}$$

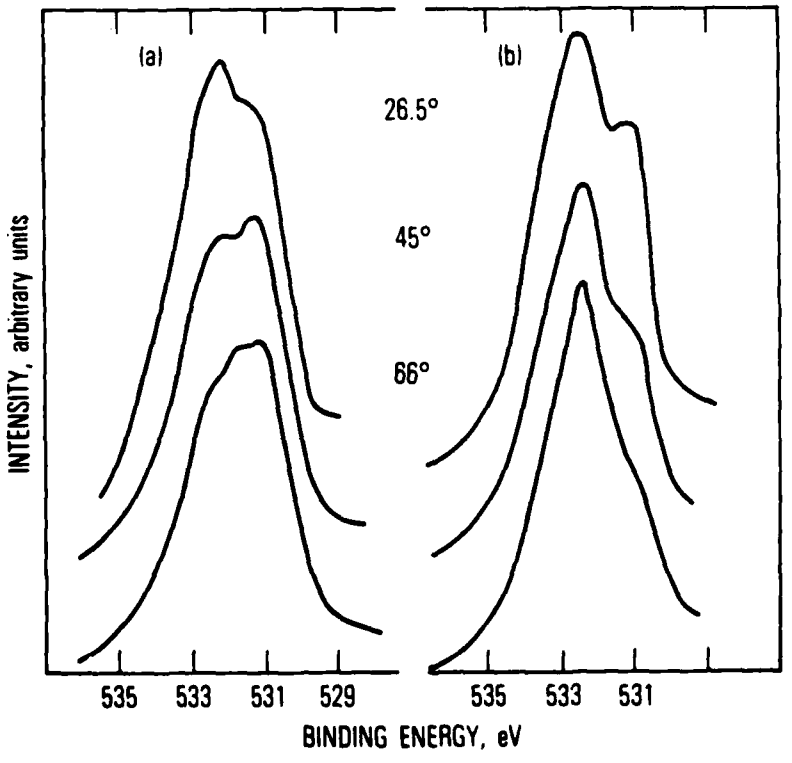


**Fig. 4. Oxygen XPS spectra at different angles for the same $MoS_2$ films as in Fig. 3: (a) Type I film; (b) Type II film.**

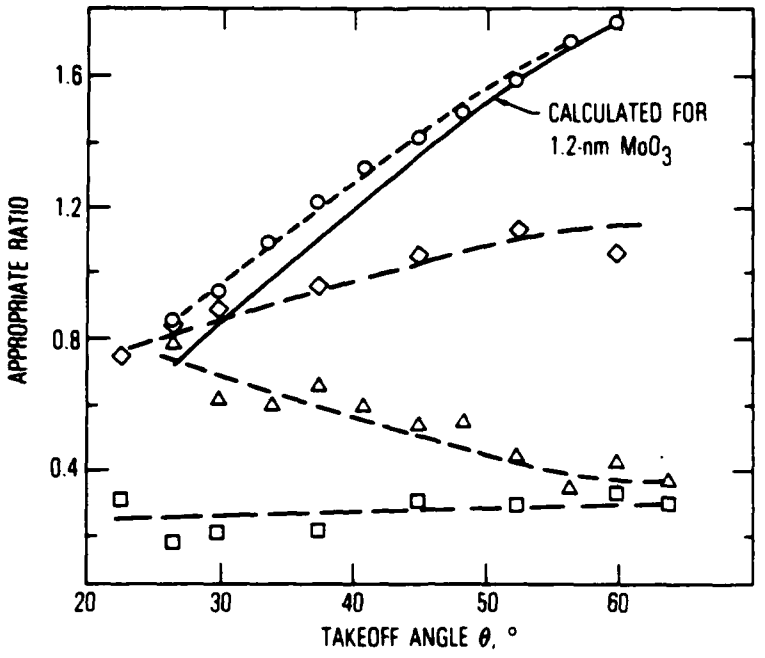


Fig. 5. Variation in Mo and O XPS peaks for 200-nm-thick sputter-deposited $MoS_2$ films as a function of takeoff analysis angle θ. See text for explanation of calculated line. $O_2$ = Mo(IV):Mo(VI) Type II; ◇ = $O^{2-}/O_2$ Type I; Δ = $O^{2-}/O_2$ Type II; □ = Mo(IV):Mo(VI) Type I.

The fit of Eq. (4) with $t_2$ = 1.2 nm to the data for the Type II film is very good, considering the model's simplicity. The deviation at the smaller takeoff angles can be attributed to less than 100 percent oxidation of the film or to the presence of voids (discontinuities) in the oxide layer, or both. That the best fit for these data corresponds to a 1.2-nm-thick oxide layer over the $MoS_2$, agrees excellently with the results of AES and XPS measurements on a variety of films at constant angle, for which calculations indicated an oxide layer 1 to 1.5 nm thick for Type II films and > 30 nm thick for Type I films.[7]

## V. LAYERING OF SULFUR AND MOLYBDENUM ATOMS

Pure molybdenite ($MoS_2$) has a hexagonal, layered crystal structure, with planes of S and Mo atoms alternating. The outermost layer for the basal surface is S atoms with a layer of Mo and then two S layers followed by another Mo layer and so forth.[12] This layered arrangement affects the relative intensities of both Auger electrons and photoelectrons emitted from the respective elements.[7,13] The measured S:Mo peak intensity ratios are much larger than the 2:1 stoichiometry would indicate, even after correcting for the standard sensitivity factors,[14] partly because the outer S layer scatters (shields) electrons emitted by the Mo atoms but is itself unshielded on a clean surface. [The layered structure of $MoS_2$ with the basal surface of sulfurs makes them very convenient materials to study by electron spectroscopy because very little adsorption of ambient gases occurs.[13,15,16]] This shielding phenomenon is accentuated when the angle of analysis of the emitted electrons is changed, just as in the case of the contaminant overlayer (oxide) discussed in the preceding section. A reduction in the takeoff angle will enhance the S signal relative to that of Mo if the surface analyzed is ordered as the single crystal. Consequently, a plot of the S:Mo peak intensity ratio versus the angle $\theta$ should show an upward curve at small values of $\theta$.

Angle-variation data for freshly cleaved $MoS_2$ crystals, presented in Fig. 6, indicate the expected increase at small $\theta$ for both the S:Mo and the O:Mo ratios, that increase confirming the supposition that both S and O have relatively high concentrations on the outermost surface of the crystal. These data can again be fit quite well by reference to Eq. (1). For the S:Mo ratio, the outer S layer will attenuate the Mo electrons and these levels will attenuate emission from lower levels. If only the outermost S and Mo layers are considered, then the Mo but not the S signal will change as a function of $\theta$, if one neglects angular variations in emission intensity caused by orbital symmetries. The intensity of the Mo emission will be given by

$$I_{Mo} = K\lambda_{Mo} \exp(-t_2/\lambda \sin \theta) [1 - \exp(-t_1/\lambda \sin \theta)] \qquad (5)$$

where $t_1$ is the thickness of the emitting Mo layer and $t_2$ that of the attenuating S layer. The ratio of Mo intensity at $\theta = 90°$ divided by that at any $\theta$ is given by

$$\frac{I_{90°}}{I_\theta} = \frac{\exp(-t_2/\lambda)}{\exp(-t_2/\lambda \sin \theta)} \qquad (6)$$

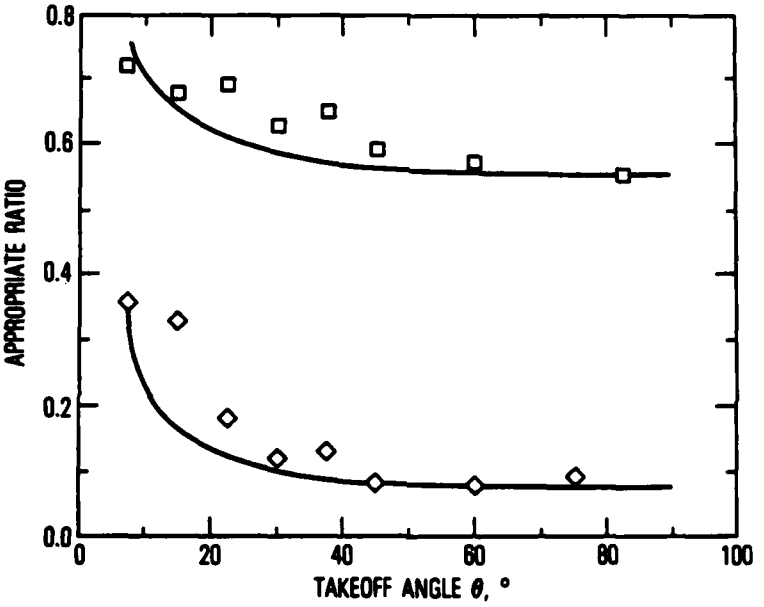


Fig. 6. Variation in S:Mo (□) and O:Mo (◇) as a function of $\theta$ for basal plane of molybdenite single-crystal substrate. Lines for fit to each data set are calculated from Eq. (6) in text.

Equation (6) was used both to produce the curve in Fig. 6 for $t_2 = 0.154$ nm, which is the Mo-S lattice spacing in molybdenite, and to fit the data for the O:Mo peak intensity ratios but with a thickness of adsorbed oxygen of 0.55 nm, indicating more than one monolayer of adsorption. The latter result contrasts to conclusions of previous studies that there was negligible $O_2$

adsorption on the basal plane of molybdenite.[15,16] However, their data show some oxygen peaks, and they made no attempt to estimate how much might be present on the surface.

The curves calculated from the simplified model of electron scattering by the outermost S or O layers on these molybdenite crystals fit those data rather well, which is somewhat surprising, especially for the S:Mo data. The calculation considers only one scattering S layer. In fact, effects due to many layers of S and Mo weighted for their thicknesses and depths beneath the surface should be summed in a multilayer scattering calculation. Such a calculation was made with the assumption that single S and Mo layers had the same thickness and scattering cross section, and the results did not fit the data as well as the single-layer model. Future work will produce more refined multilayer calculations that will vary the effective layer thicknesses of S and Mo to establish whether the fit to the data can be improved. The calculation that yielded the oxygen layer thickness of 0.55 nm first assumed shielding of the Mo emission by a single S layer and then determined the amount of oxygen needed to best fit the O:Mo data. No claim is made concerning the chemistry of the oxygen species beyond the fact that it is adsorbed over the S of $MoS_2$. It could be molecular $O_2$ or adsorbed $H_2O$, but clearly no oxidation of either $S^{2-}$ or Mo(IV) in the crystal could be detected. [It turns out to be unnecessary to include the oxygen layer in the S:Mo calculations because the oxygen shields both the S and Mo signals and cancels algebraically in the derivation of Eq. (6).]

## VI. ORIENTATION OF SPUTTERED $MoS_2$ FILMS

An attempt was made to obtain sputtered films oriented, throughout their depth and at the film-substrate interface, in a configuration with their basal plane parallel to the substrate surface plane, by depositing the $MoS_2$ onto an already oriented substrate: slices of molybdenite crystal. Highly polished stainless-steel substrates were placed adjacent to the single-crystal substrates during depositions to obtain films prepared under identical conditions on each surface. Very thin films (4-20 nm thick) were prepared to examine the interface region between film and substrate.

Results for a 4.3-nm-thick film on the molybdenite crystal are shown in Figs. 7 and 8. The shapes of the Mo peaks (Fig. 7; i.e., the full widths at half maxima) compared with those for the bare substrate (Fig. 2) evince the inferior crystallinity of the films and indicate that some oxidation of the films has occurred. However, the increase in the S:Mo ratio with decreasing $\theta$ indicates that some orientation of the crystallites of deposited films persists. Data for the S:Mo ratio for unoriented films, those deposited on the steel substrates, ranged between 0.95:1 and 1:1 with no trend in terms of takeoff angle. A good fit to the data for the thin film on molybdenite for S:Mo variation is obtained if the multilayer scattering calculation is used. However, there is deviation at near-grazing angles (see the solid line in Fig. 8).

The O:Mo ratio also changes with $\theta$ much like the single-crystal data. However, for the thin film there is more than a twofold increase in the relative oxygen signal (compared with the crystal substrate) and there is a substantial fraction of oxide signal (as opposed to adsorbed oxygen species) that shows a relative increase as $\theta$ approaches 90°. This behavior is like that shown in Fig. 5 for the 200-nm-thick Type I films, on which a layer of adsorbed oxygen species overlaid the oxide layer. In contrast to the Type I films, though, the variation in the Mo(IV) and Mo(VI) peaks shows an opposite trend; that is, there is relatively more Mo(IV) ($MoS_2$) at the outer surface of the thin film. The probable explanation of this result is that there is a

layer of oxide between the substrate surface and the thin film that was formed during the initial stages of deposition. Even though a shutter is used to condition the sputtering target before deposition, some oxygen must be present when the shutter is first opened and reacts to form a thin oxide layer that is gradually covered with $MoS_2$. As sputtering continues, the sulfide deposition predominates and the relative amount of Mo(IV) exceeds 90 percent of the total Mo. Analyses of slightly thicker films (8 and 16 nm thick) do not show these trends in Mo and O signals with θ, confirming this explanation; emission from the interfacial oxide layer is totally shielded by the thicker $MoS_2$ films.

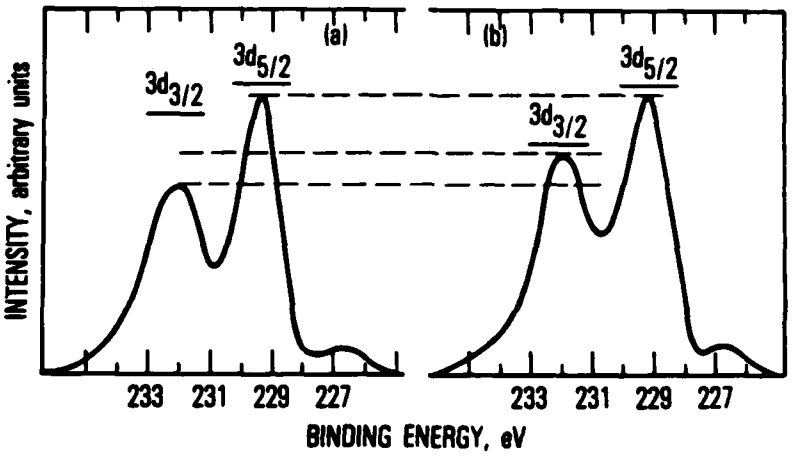


Fig. 7. Molybdenum XPS spectra at different angles for 4.3-nm-thick $MoS_2$ film on molybdenite crystal substrate: (a) θ = 7.5°, Mo(IV):Mo(VI) ≈ 13; (b) θ = 60°, Mo(IV):Mo(VI) ≈ 6.

The 4.3-nm-thick film of $MoS_2$ on the steel substrate also indicates the presence of an oxide layer between the film and substrate, which was expected because the substrate had an oxide layer prior to deposition. The spectra of this film did not show any significant variation in S:Mo with θ, indicating that either the film crystallites are not oriented on the steel surface or the steel surface is too rough for the small variations within the film to be measurable.

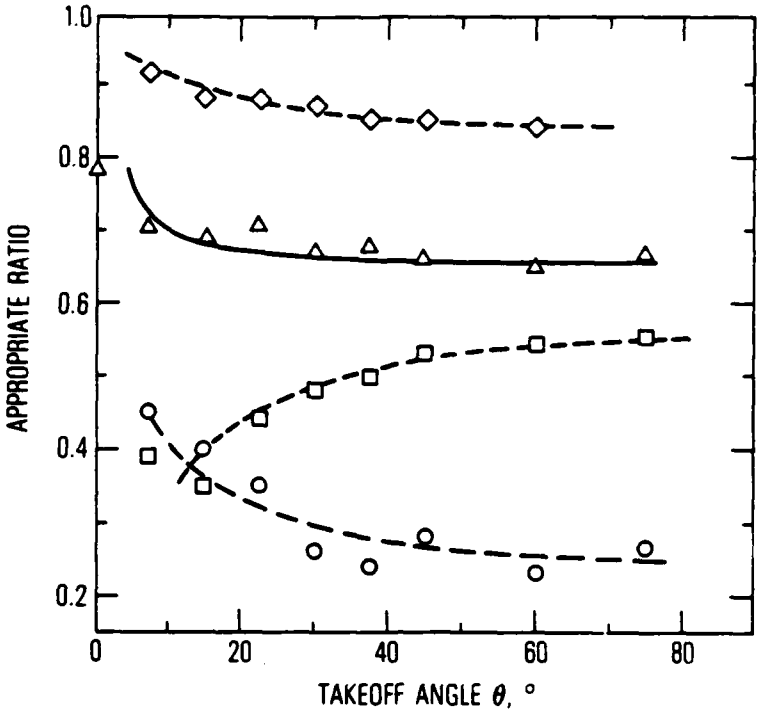


Fig. 8. Variation in fraction of Mo(IV) (◇), S:Mo(△), fraction of $O^{2-}$ (□), and O:Mo (○) as a function of θ for 4.3-nm-thick $MoS_2$ film on molybdenite crystal. The solid line for the S:Mo data was calculated using Eq. (6).

## VII. CONCLUSIONS

The preliminary results of angle-dependent XPS measurements together with electron scattering calculations demonstrate that it is possible to detect orientation of sputtered $MoS_2$ films, when it occurs, and also to assess oxidation processes both during the deposition process and subsequently, when the film is exposed to various environments. Careful analysis of the angle-dependent data provides composition, structure, and depth information beyond that attainable with constant-angle measurements. Present results show (1) the presence of a 1.2-nm-thick $MoO_3$ layer on the outer surface of 200-nm-thick Type II $MoS_2$ films; (2) the presence of a much thicker $MoO_3$ layer on Type I films; (3) the layering of Mo and S atoms within the basal planes of molybdenite crystals; (4) the presence of multilayer (2-3 layer) adsorption of oxygen-containing species on the basal surface of molybdenite: (5) the planar orientation of very thin (4.3-nm) sputter-deposited $MoS_2$ films on molybdenite substrates; and (6) the formation of an oxide layer during the initial stages of sputter deposition of $MoS_2$ films. Further work is required to obtain thicker films that are oriented at the substrate interface and throughout the bulk layers, and to eliminate the interfacial oxidation during the deposition.

## REFERENCES


1. Spalvins, T., "Tribological Properties of Sputtered $MoS_2$ Films in Relation to Film Morphology," Thin Solid Films 73, 291-297 (1980).

2. Wheeler, D. R., "Application of ESCA to the Determination of Stoichiometry in Sputtered Coatings and Interface Regions," NASA Tech. Memo NASA TM-78896 (1978).

3. Christy, R. I., and Ludwig, H. R., "RF Sputtered $MoS_2$ Parameter Effects on Wear Life," Thin Solid Films 64, 223-229 (1979).

4. Stupp, B. C., "Synergistic Effects of Metals Co-Sputtered with $MoS_2$," Thin Solid Films 84, 257-266 (1981).

5. Fleischauer, P. D., "Effects of Crystallite Orientation on Environmental Stability and Lubrication Properties of Sputtered $MoS_2$ Thin Films," ASLE Trans. 27, 82-88 (1984).

6. Stewart, T. B., and Fleischauer, P. D., "Chemistry of Sputtered Molybdenum Disulfide Films," Inorg. Chem. 21, 2426-2431 (1982).

7. Fleischauer, P. D., and Stewart, T. B., "Chemistry of Sputtered Molybdenum Disulfide Films. II. Crystallite Orientation Effects," submitted to Inorg. Chem., 1983.

8. Bertrand, P. A., Kalinowski, W. J., Tribble, L. E., and Tolentino, L. U., "Fast Optical Position-Sensitive Detector for McPherson ESCA-36," Rev. Sci. Instrum. 54, 387-389 (1983).

9. Fadley, C. S., "Basic Concepts of X-ray Photoelectron Spectroscopy," in Electron Spectroscopy: Theory, Techniques and Applications, Brundle, C. R., and Baker, A. D. (eds.), Academic Press, New York (1978), Vol.2, p. 1.

10. Phillips, L. V., Salvati, L., Carter, W. J., and Hercules, D. M., "Some Aspects of Quantitative Surface Analysis by Electron Spectroscopy for Chemical Analysis," in Quantitative Surface Analysis of Materials, McIntyre, N. S. (ed.), ASTM STP 643 (1977), p. 47.

11. See, for example, Sham, T. K., and Lazarus, M. S., "X-ray Photoelectron Spectroscopy (XPS) Studies of Clean and Hydrated $TiO_2$ (Rutile) Surfaces," Chem. Phys. Lett. 68, 426-432 (1979).

12. Jamison, W. E., "Structure and Bonding Effects on the Lubricating Properties of Crystalline Solids," ASLE Trans., 15, 296-305 (1972).

13. Matsunaga, M., Homma, T., and Tanaka, A., "Investigation of Vapor Adsorption on Molybdenum Disulfide Surfaces by Auger Electron Spectroscopy," ASLE Trans. 25, 323-328 (1982).

14. Handbook of Auger Electron Spectroscopy, Perkin-Elmer Corp., Physical Electronic Division, Eden Prairie, Minnesota (1976).

15. Salmeron, M., Somorjai, G. A., Wold, A., Chianelli, R., and Liang, K. S., "The Adsorption and Bonding of Thiophene, Butene, and $H_2S$ on the Basal Plane of $MoS_2$ Single Crystals," Chem. Phys. Lett. 90, 105-107 (1982).

16. Suzuki, K., Soma, M., Onishi, T., and Tamaru, K., "Reactivity of Molybdenum Disulfide Surfaces Studied by XPS," J. Electron Spectrosc. Relat. Phenom. 24, 283-287 (1981).

## LABORATORY OPERATIONS

The Laboratory Operations of The Aerospace Corporation is conducting experimental and theoretical investigations necessary for the evaluation and application of scientific advances to new military space systems. Versatility and flexibility have been developed to a high degree by the laboratory personnel in dealing with the many problems encountered in the nation's rapidly developing space systems. Expertise in the latest scientific developments is vital to the accomplishment of tasks related to these problems. The laboratories that contribute to this research are:

Aerophysics Laboratory: Launch vehicle and reentry aerodynamics and heat transfer, propulsion chemistry and fluid mechanics, structural mechanics, flight dynamics; high-temperature thermomechanics, gas kinetics and radiation; research in environmental chemistry and contamination; cw and pulsed chemical laser development including chemical kinetics, spectroscopy, optical resonators and beam pointing, atmospheric propagation, laser effects and countermeasures.

Chemistry and Physics Laboratory: Atmospheric chemical reactions, atmospheric optics, light scattering, state-specific chemical reactions and radiation transport in rocket plumes, applied laser spectroscopy, laser chemistry, battery electrochemistry, space vacuum and radiation effects on materials, lubrication and surface phenomena, thermionic emission, photosensitive materials and detectors, atomic frequency standards, and bioenvironmental research and monitoring.

Electronics Research Laboratory: Microelectronics, GaAs low-noise and power devices, semiconductor lasers, electromagnetic and optical propagation phenomena, quantum electronics, laser communications, lidar, and electro-optics; communication sciences, applied electronics, semiconductor crystal and device physics, radiometric imaging; millimeter-wave and microwave technology.

Information Sciences Research Office: Program verification, program translation, performance-sensitive system design, distributed architectures for spaceborne computers, fault-tolerant computer systems, artificial intelligence, and microelectronics applications.

Materials Sciences Laboratory: Development of new materials: metal matrix composites, polymers, and new forms of carbon; component failure analysis and reliability; fracture mechanics and stress corrosion; evaluation of materials in space environment; materials performance in space transportation systems; analysis of systems vulnerability and survivability in enemy-induced environments.

Space Sciences Laboratory: Atmospheric and ionospheric physics, radiation from the atmosphere, density and composition of the upper atmosphere, aurorae and airglow; magnetospheric physics, cosmic rays, generation and propagation of plasma waves in the magnetosphere; solar physics, infrared astronomy; the effects of nuclear explosions, magnetic storms, and solar activity on the earth's atmosphere, ionosphere, and magnetosphere; the effects of optical, electromagnetic, and particulate radiations in space on space systems.


DATE
ILME